Incommensurate Spin Density Wave in Metallic $V_{2-y}O_3$

Wei Bao,[1] C. Broholm,[1,2] S. A. Carter,[3] T. F. Rosenbaum,[3] G. Aeppli,[4]
S. F. Trevino,[2,5] P. Metcalf,[6] J. M. Honig,[6] and J. Spalek[6]

[1] The Johns Hopkins University, Baltimore, Maryland 21218
[2] National Institute of Standards and Technology, Gaithersburg, Maryland 20899
[3] The University of Chicago, Chicago, Illinois 60637
[4] AT&T Bell Laboratories, Murray Hill, New Jersey 07974
[5] ARDEC, Picatinny Arsenal, New Jersey 07806
[6] Purdue University, West Lafayette, Indiana 47907

We show by neutron diffraction that metallic $V_{2-y}O_3$ develops a spin density wave below $T_N \approx 9$ K with incommensurate wave vector $\mathbf{q} \approx 1.7c^*$ and an ordered moment of $0.15\mu_B$. The weak ordering phenomenon is accompanied by strong, nonresonant spin fluctuations with a velocity $c = 67(4)$ meV Å. The spin correlations of the metal are very different from those of the insulator and place $V_{2-y}O_3$ in a distinct class of Mott-Hubbard systems where the wave vector for magnetic order in the metal is far from a high symmetry commensurate reciprocal lattice point.

In the canonical Mott-Hubbard system, where the Coulomb interactions between electrons lead to a spectacular breakdown of the conventional band theory of solids, doping transforms an insulating antiferromagnet into a highly correlated metal. For selected copper oxides, the metal can superconduct while in $V_{2-y}O_3$ it is a strongly renormalized Fermi liquid [1] with a large linear specific heat ($\gamma = 54$ mJ/mol K^2 V), a large Pauli paramagnetic susceptibility, χ_0, and a T^2 term in the electrical resistivity [2]. In response to experiments on $V_{2-y}O_3$ and its derivatives, Brinkman and Rice developed a mean-field theory which accounts for the large effective carrier mass and therefore the enhanced γ and χ_0 near the metal-insulator transition (MIT) [3]. They did not consider magnetic order in the metal, a possibility revealed by more recent theories [4], with profound consequences for transport and thermodynamic properties. Thus far, searches for static order of this type in the cuprates have not succeeded. However, in the present work we demonstrate that such order actually does exist in $V_{2-y}O_3$ for small y (≤ 0.05). Furthermore, our neutron scattering experiments show that the ordering and associated fluctuations whose amplitude is much larger than the ordered moment, are different from the ordering and spin waves in the undoped insulator [5].

We grew single crystals of $V_{2-y}O_3$ using a skull melter [6]. The cation deficiency was controlled to within $\delta y = 0.003$ by annealing 2 mm thick slabs for two weeks at 1400 °C in a CO-CO_2 atmosphere [7]. Four single crystals with a total volume of 7 cm^3 were sliced into comb shapes prior to annealing for use in the inelastic experiments. We index wave-vector transfer in the hexagonal reciprocal lattice with $a^* = 4\pi/\sqrt{3}a = 1.4700(4)$ Å^{-1} and $c^* = 2\pi/c = 0.4484(1)$ Å^{-1}. To within the quoted error bars, the lattice parameters are independent of doping for $0.017(3) \leq y \leq 0.037(4)$. The neutron scattering experiments were carried out on pyrolytic-graphite-based thermal neutron triple axis spectrometers at NIST with

samples mounted in the (hhl) and $(h0l)$ zones. High pressure neutron diffraction was performed using a maraging steel cell with ^{4}He as the pressure transducing medium.

We first characterized the low temperature ($T = 1.4$ K) antiferromagnetic phase in metallic $V_{2-y}O_3$ [2,8]. Antiferromagnetic Bragg peaks were not found at $(\frac{1}{2}\frac{1}{2}0)$, corresponding to the ordered structure of the insulator, but instead appeared as pairs at incommensurate positions $(h0l \pm \delta)$ with $\delta \approx 1.7$ and for $l - 4h = 6n$. In Fig. 1 we show the incommensurate peaks corresponding to $(10\overline{2} + \delta)$ and $(104 - \delta)$ from which we find $\delta = 1.700(2)$ for $y = 0.037(4)$. The peaks are resolution limited placing a lower limit of 10^3 Å on the correlation length, ξ. Extensive searches along high symmetry directions in the $(h0l)$ zone revealed no other temperature dependent Bragg peaks. These observations imply the presence of a static spin configuration which may be described as $\mathbf{S_{R,d}} = S_x \hat{\mathbf{x}} \cos(\mathbf{q} \cdot \mathbf{R} + \varphi_d) + S_y \hat{\mathbf{y}} \sin(\mathbf{q} \cdot \mathbf{R} + \varphi_d)$, where $\hat{\mathbf{x}}$ and $\hat{\mathbf{y}}$ are orthogonal unit vectors and $\mathbf{R}$ is a Bravais lattice vector. In order to determine the phases ϕ_d of the four magnetic ions within a primitive unit cell and the size of the ordered moment, we measured the integrated intensities of 13 magnetic satellites. Absolute units were derived by normalizing to 22 nuclear Bragg peaks. We first compare the data to the helimagnetic spin configuration $|S_x| = |S_y|$ which satisfies the requirements that the static spin densities associated with each vanadium ion have equal magnitude and that spins of equivalent pairs form the same angles with each other. As shown in Fig. 2, the primitive rhombohedral unit cell contains four vanadium ions displaced along the threefold $\mathbf{c}$ axis, thus forming two inequivalent pairs [9]. Denoting by $\Delta\psi_1$ and $\Delta\psi_2$ the phase shifts or angles between spins of these pairs, the phase shift between spins separated by $\mathbf{c}$ is $\mathbf{q} \cdot \mathbf{c} = 2(\Delta\psi_1 + \Delta\psi_2)$. Since $\mathbf{q} \cdot \mathbf{c} = 2\pi\delta$ is known from the location of the magnetic Bragg peaks, the assumptions leave just a single phase to be extracted from the intensity data. Expressing the phases φ_{di} in terms of $\Delta\psi_1$
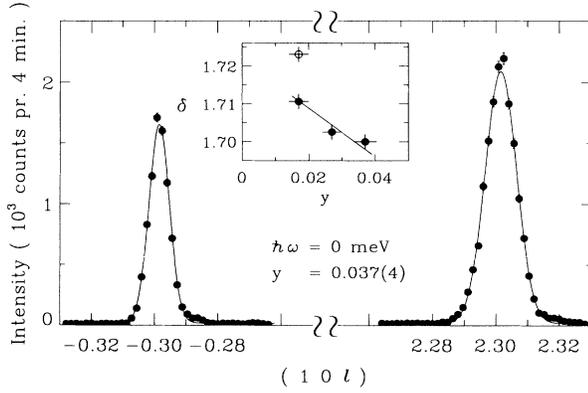
FIG. 1. Scans along $\mathbf{c}^*$ through antiferromagnetic Bragg peaks in $V_{2-y}O_3$ for $y = 0.037(3)$ at $P = 0$, $T = 1.4$ K. Collimations were $20'\text{-}10'\text{-}10'$ $E_i=14.76$ meV and no analyzer was used. The solid lines are Gaussians with widths given by the instrumental resolution. The inset shows the y dependence of the incommensurate wave vector $\mathbf{q} = \delta\mathbf{c}^*$. The open circle indicates the position of an additional incommensurate peak which appears for $T < 6$ K in the $y = 0.017(3)$ sample. At present it is unclear whether this peak is the order parameter of an additional intrinsic phase in the vicinity of the MIT or results from sample inhomogeneities.

we have $\varphi_{d1} = 0$, $\varphi_{d2} = \Delta\psi_1$, $\varphi_{d3} = (\Delta\psi_1 + \Delta\psi_2) = \frac{1}{2}\mathbf{q}\cdot\mathbf{c}$, and $\varphi_{d4} = \frac{1}{2}\mathbf{q}\cdot\mathbf{c} + \Delta\psi_1$. The best fit for a $y = 0.027(3)$ sample was obtained with spins in the basal plane of magnitude $M_q = g\mu_B S_\alpha = 0.148(7)\mu_B$ and $\Delta\psi_1 = 1.43(7)\pi$. Although diffraction cannot distinguish the helimagnetic configuration ($|S_x| = |S_y|$) from amplitude modulated structures ($|S_x| \neq |S_y|$) with equivalent phases, ϕ_{di}, only in the former case is there a physical argument for the phase relations imposed. The excellent agreement between the simple model and data to which Table I testifies therefore lends support to the identification of the ordered structure as a transverse helimagnet or SDW. The resulting spin configuration is depicted in Fig. 2. Note that the angle between neighboring spins in a plane is $\Delta\psi_1 - \mathbf{q}\cdot\mathbf{c}/6 = 0.86(7)\pi$ so each plane is close to being a perfect planar honeycomb antiferromagnet and spins in nearest neighbor planes are almost perpendicular since $\Delta\psi_1 \approx 3\pi/2$.

We show in Fig. 3 the temperature dependence of the staggered magnetization for $V_{2-y}O_3$ with $y = 0.017(3)$. It is apparent that $T_N = 10$ K, and that the growth in M_q is roughly consistent with conventional weak coupling BCS mean field theory. The behavior of M_q closely parallels that of the resistivity (also shown in Fig. 3 less a paramagnetic background), even displaying similar rounding near T_N due to critical fluctuations. The solid line through the resistivity data is the behavior expected due to the opening of a gap with the temperature dependence predicted by the BCS gap equation [10] and taking $\Delta \approx k_B T_N$.

To understand the relation of the metallic spin correlations to the MIT, we have studied these as a func-
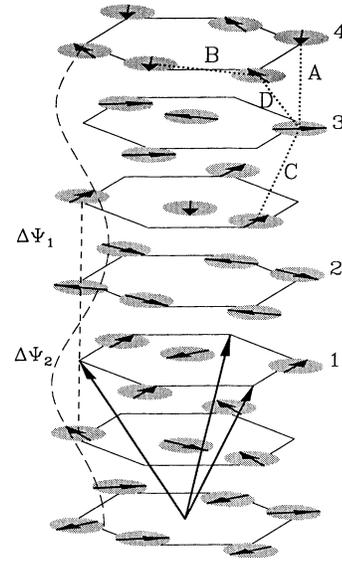
FIG. 2. Incommensurate spin structure in $V_{2-y}O_3$. Macroscopically both spiral handednesses exist in our crystals. Numbers 1–4 indicate the basis of the rhombohedral unit cell. A,B and C,D indicate relevant direct and superexchange paths, respectively.

tion of hydrostatic pressure and vacancy doping. We plot in Fig. 4 an overview of the phase diagram so obtained. The SDW is the low temperature, low pressure phase throughout the range of doping required to suppress the monoclinic insulating phase. Pressure reduces both T_N and the staggered magnetization, M_q, and linear extrapolation would predict an upper critical pressure varying from 10 ± 3 kbar for $y = 0.017(3)$ to 18 ± 3 kbar for $y = 0.027(3)$, somewhat less than the 20 to 26 kbar required to suppress the insulating phase of the stoichiometric $y = 0$ compound. While T_N, M_q, and $\Delta\rho/\rho$ all decrease substantially with doping and pressure, the incommensurate wave vector $\mathbf{q}$ varies by less

TABLE I. Comparison of the magnetic Bragg scattering cross sections, σ_{obs}, for $V_{1.973}O_3$ to a transverse SDW model with $\sigma_{cal}(\mathbf{Q}) = (\gamma r_0/2)^2 M_q^2(1+|\hat{\mathbf{Q}}\cdot\hat{\mathbf{c}}|^2)|f(\mathbf{Q})|^2|\mathcal{F}(\mathbf{Q})|^2$, where $(\gamma r_0/2)^2 = 72.65 \times 10^{-3}$ b/μ_B^2, $M_q = 0.148(7)\mu_B$ per V ion, f is the magnetic form factor, and the normalized magnetic structure factor for one hexagonal unit cell, $\mathcal{F}$, was calculated for $\Delta\Phi_1 = 1.43\pi$. The resulting reliability coefficient $R = \sum|\sigma_{obs} - \sigma_{cal}|/\sum\sigma_{obs}$ is 14%.

$\mathbf{Q}$	σ_{obs}[a]	σ_{cal}[a]	$\mathbf{Q}$	σ_{obs}[a]	σ_{cal}[a]
(0 0 7.7)	14.6(7)	12.2	(1 0 $\overline{6.3}$)	22(2)	22.8
(0 0 4.3)	0.9(5)	0.9	(1 0 $\overline{9.7}$)	5(1)	5.0
(1 0 8.3)	5.3(4)	3.7	(2 0 6.3)	6.6(4)	8.1
(1 0 5.7)	4.3(3)	3.4	(2 0 3.7)	13.4(4)	14.2
(1 0 2.3)	43.9(9)	37.5	(2 0 0.3)	8.1(5)	9.2
(1 0 $\overline{0.3}$)	25.9(6)	23.3	(2 0 $\overline{2.3}$)	10.6(8)	12.6
(1 0 $\overline{3.7}$)	52(1)	43.9			

[a]In units of 10^{-3} b per hexagonal unit cell.
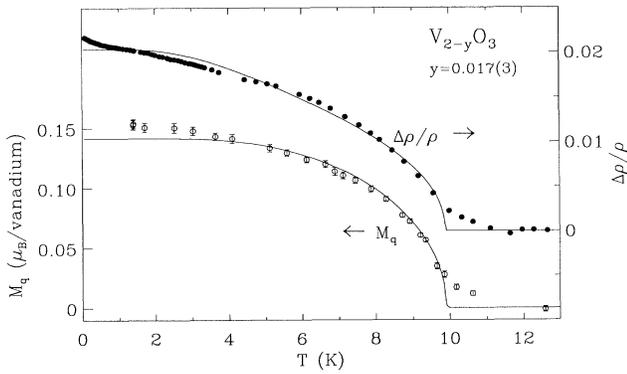
FIG. 3. Temperature dependence of the staggered magnetization, M_q, and excess resistivity in the SDW phase: $\Delta\rho/\rho = (\rho - AT^2)/\rho$ with A chosen so $\Delta\rho/\rho \to 0$ for $T > T_N$. Solid lines are model calculations described in the text. M_q was measured by neutron scattering with $E_f = 14.7$ meV and collimations $40'$-$48'$-$48'$-$40'$.

FIG. 4. Phase diagram for $V_{2-y}O_3$. The first-order phase boundary to the antiferromagnetic monoclinic insulating state AFI was obtained from Ref. [1]. The SDW phase boundary was determined by resistivity measurements (filled symbols) and neutron diffraction (open symbols).

than $0.01c^* = 4.5 \times 10^{-3}$ Å^{-1} for $0 < P < 8$ kbar and $0.013(3) \leq y \leq 0.037(4)$. More accurate measurements at $P = 0$ (inset of Fig. 1) , however, demonstrate that q for $y = 0.017(3)$ is distinguishable from that for $y = 0.027(3)$ and $0.037(4)$.

Having described the static ordering in $V_{2-y}O_3$, we turn to the low temperature magnetic fluctuations of the metal for $y = 0.027(3)$. We show in Fig. 5 inelastic magnetic scattering as a function of wave vector transfer, κ, at three different energies. Even at energies $\hbar\omega$ more than an order of magnitude beyond $k_B T_N$, the inelastic scattering is strongly peaked when κ is close to the position of a magnetic satellite, $Q = \tau \pm q$. The dashed lines show the intensity distribution to which conventional antiferromagnetic spin waves with a velocity $c = 130$ meV Å would give rise with the spectrometer resolution of our experiments [11]. Clearly this model cannot account for the magnetic excitations and our resolution is adequate to conclude that for $1.5 \leq \hbar\omega \leq 18$ meV, the dynamic spin correlation function consists of a single ridge as a function of energy centered near each incommensurate magnetic zone center [12]. At low energies the peak centers and relative intensities are indistinguishable from those of the incommensurate magnetic Bragg peaks (Fig. 1). At higher energies, however, the peak centers move towards the commensurate antiferromagnetic Bragg point (101), analogous to the transverse SDW phase of chromium [13]. The inset shows that the resolution corrected Gaussian width σ_ω of these peaks [14] grows with $\hbar\omega$. The inverse slope of $67(4)$ meV Å is a characteristic velocity for propagation of spin fluctuations in the metal. The finite intercept of σ_ω as $\hbar\omega \to 0$ corresponds to a correlation length of $14(4)$ Å for low frequency spin fluctuations which is much less than the static correlation length, $\xi > 10^3$ Å implying that the spin fluctuations are not conventional spin waves. This is also apparent from the fact that the energy integrated
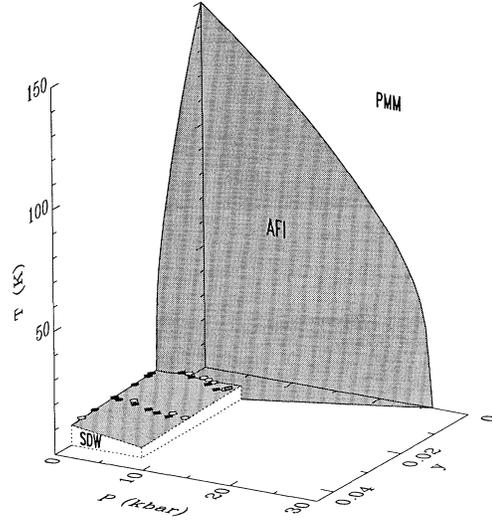
inelastic cross section for $\hbar\omega \leq 18$ meV (which may be far below the true bandwidth) and $\kappa \approx (102.3)$ is $0.20(5)$ b/hexagonal unit cell, exceeding that of the corresponding antiferromagnetic Bragg peak (Table I) by a factor 5. Scaling the static ordered moment by the square root of this factor, we obtain an estimate of $0.32(8)\mu_B$ for the total fluctuating moment in this energy range; an appreciable fraction of the total spin associated with atomic $S = 1$ V^{3+}: $g\mu_B\sqrt{S(S+1)} = 2.8\mu_B$.

We have shown that metallic $V_{2-y}O_3$ undergoes small moment incommensurate magnetic ordering at low temperatures and pressures. In addition, the magnetic fluctuations are both substantially larger in amplitude than the ordered moment, and in bandwidth than the ordering temperatures. Finally, the resistivity rises in order-parameter-like fashion below T_N, and scales with the incommensurate magnetization rather than the magnetic critical fluctuations, as in local moment systems. These facts distinguish $V_{2-y}O_3$ from the isostructural but insulating solid solutions $(Cr_{1-x}Fe_x)_2O_3$, where incommensurate antiferromagnetic order results from competing exchange [15,16]. The magnetic properties are more reminiscent of classic itinerant antiferromagnetism of the type found in Cr and its alloys. Indeed, transport, neutron and specific heat [1] measurements give similar estimates for the small fractional area A_m/A of the Fermi surface involved in the SDW for $y \approx 0.03$: $(A_m/A)_\rho = (\Delta\rho/\rho)_{T=0} = 0.02$, $(A_m/A)_{M_q} = (M_q/2\mu_B)_{T=0} = 0.075$, $(A_m/A)_C = \Delta C/1.43C(T_N) = 0.080$. For SDW antiferromagnets the velocity of long wavelength spin fluctuations is of the order of the Fermi velocity on the relevant parts of the Fermi surface [17]. Comparison of the spin wave velocities, $67(4)$ meV Å for $V_{2-y}O_3$ and 0.9 eV Å for
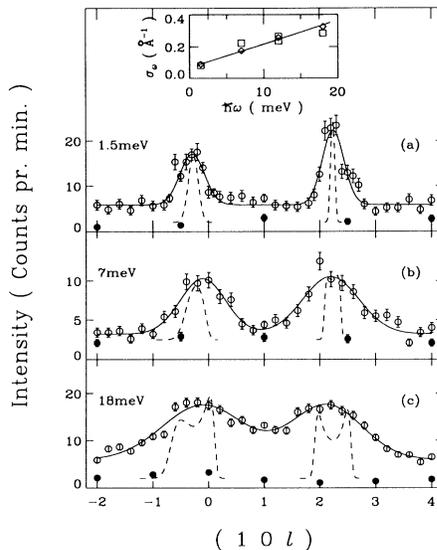
FIG. 5. Constant energy scans at $T = 1.5$ K for $V_{2-y}O_3$, $y = 0.027(3)$ through two incommensurate magnetic zone centers. Filled symbols indicate the analyzer turned background. Dashed lines show the calculated response of our instrument for spin wave excitations with a velocity $c = 130$ meV Å. Solid lines are Gaussian fits. The inset shows the energy dependence of the resolution-corrected widths of constant energy scans. In (a) and (b) $E_f = 13.7$ meV and horizontal collimations were 60'-40'-40'-40', whereas in (c) $E_i = 35$ meV and collimations were 60'-40'-60'-60'. Vertical collimations were 300'-170'-230'-970'.

Cr indicates that in $V_{2-y}O_3$ we are dealing with an instability involving heavy quasiparticles, as one might expect given the large Sommerfeld constant of metallic $V_{2-y}O_3$. The corresponding Fermi surface is large, with an area $A = 4\pi^3 \hbar v_f g(\epsilon_f) = 7.9$ Å^{-2}, implying a carrier density of 0.4 per vanadium, far exceeding the vacancy density but of the same order as the hole density of 0.45 which may be extracted from the low temperature Hall effect [18]. The large Fermi surface implies that nesting vectors, and hence incommensurate magnetic ordering vectors, cannot change rapidly with doping. In particular, assuming a uniform Fermi velocity and equality between changes in the vacancy and carrier densities, the linear dimension of the Fermi surface changes by $\Delta k = \Delta y 4\pi^3 / A v_0$ when the vacancy density changes by $\Delta y / v_0$. Thus, one would expect the incommensurate wave vector to change by 0.006 Å^{-1} = 0.0128c^* over the range of compositions $\Delta y = 0.02$ probed in the present experiment. This Δq is similar to the variance actually observed (see inset of Fig. 1). While our method of calculating $\Delta q / \Delta y$ is crude, it accounts for the much more rapid variation of magnetic nesting vectors in $Cr_{1-x}V_x$ ($\Delta q / \Delta x = -2.4$ Å^{-1}) and $La_{2-x}Sr_xCuO_4$ ($\Delta q / \Delta x = 1.2$ Å^{-1}) [19].

In summary, we have discovered and characterized incommensurate magnetic order in metallic $V_{2-y}O_3$. The

ordered moment and Néel temperatures are small, while the magnitude and bandwidth of incommensurate spin fluctuations are large. Contrary to the SDW phase in the vicinity of the MIT on a square lattice such as $La_{2-x}Sr_xCuO_4$ [19], the incommensurate wave vector in the SDW phase of $V_{2-y}O_3$ is not close to a high symmetry commensurate point.

[1] D. B. McWhan et al., Phys. Rev. B 7, 326 (1973); 7, 1920 (1973).

[2] S. Carter et al., Phys. Rev. Lett. 67, 3440 (1991); S. A. Shivashanker and J. M. Honig, Phys. Rev. B 28, 5695 (1983).

[3] W. F. Brinkman and T. M. Rice, Phys. Rev. B 2, 4302 (1970).

[4] B. I. Shraiman and E. D. Siggia, Phys. Rev. Lett. 62, 1564 (1989); C. L. Kane et al., Phys. Rev. B 41, 2653 (1990); H. R. Krishnamurthy et al., Phys. Rev. Lett. 64, 950 (1990).

[5] W. B. Yelon et al., Phys. Rev. B 24, 1818 (1981).

[6] J. E. Keem et al., Am. Ceram. Soc. Bull. 56, 1022 (1977); H. R. Harrison, R. Aragon, and C. J. Sandberg, Mater. Res. Bull. 15, 571 (1980).

[7] S. A. Shivashankar et al., J. Electrochem. Soc. 128, 2472 (1981); 129, 1641 (1982).

[8] Y. Ueda et al., Mater. Res. Bull. 12, 87 (1977); Y. Ueda et al., J. Phys. Chem. Solids 39, 1281 (1978).

[9] W. R. Robinson, Acta Crystallogr. Sect. B 31, 1153 (1975).

[10] D. B. McWhan and T. M. Rice, Phys. Rev. Lett. 19, 846 (1967).

[11] N. D. Chesser and J. D. Axe, Acta Crystallogr. Sect. A 29, 160 (1973).

[12] Similar spin correlations exist in Cr near T_N: B. H. Grier, G. Shirane, and S. A. Werner, Phys. Rev. B 31, 2892 (1985), and in $La_{2-x}Ba_xCuO_4$: S. M. Hayden et al., Phys. Rev. Lett. 66, 821 (1991).

[13] C. R. Fincher, G. Shirane, and S. A. Werner, Phys. Rev. B 24, 1312 (1981).

[14] σ_ω^2 is the Gaussian variance.

[15] D. E. Cox, W. J. Takei, and G. Shirane, J. Phys. Chem. Solids 24, 405 (1963).

[16] F. Bertaut, Comput. Rend. Acad. Sci. 252, 252 (1961); Proceedings of the International Conference, Nottingham, 1964 (unpublished); N. Menyuk and K. Dwight, J. Phys. Chem. Solids 25, 1031 (1964).

[17] J. B. Sokoloff, Phys. Rev. 185, 770 (1969); 185, 783 (1969).

[18] S. A. Carter et al. (unpublished).

[19] S-W. Cheong et al., Phys. Rev. Lett. 67, 1791 (1991).